Journal of Materials Chemistry C

RSC Publishing

PAPER

View Article Online
View Journal

Cite this: DOI: 10.1039/c2tc00591c

Mechanochemical synthesis of a fluorenone-based metal organic framework with polarized fluorescence: an experimental and computational study†

Dongpeng Yan,* Rui Gao, Min Wei, Shuangde Li, Jun Lu, David G. Evans and Xue Duan

The regular assembly of organic chromophores into ordered supramolecular solids has received much attention for developing high-performance luminescent materials. Herein, a fluorenone-containing dicarboxylate (FDC) has been organized into a metal organic framework (MOF) with zinc as the metal cation by a facile mechanochemical synthesis method. The obtained Zn–FDC MOF features a pillared structure, in which the fluorenone chromophore units exhibit a highly ordered arrangement. Compared with the pristine FDC sample, the Zn–FDC MOF presents blue-shifted emission, as well as enhanced photoluminescence quantum yield and fluorescence lifetime, demonstrating the ordered arrangement of the FDC within the MOF is beneficial for the improvement of the photo-related properties of the organic chromophore. Moreover, the Zn–FDC MOF film exhibits well-defined polarized photoemission with a polarized anisotropy of 0.10–0.15. Periodic density functional theoretical (DFT) calculations illustrate that no energy/electronic transfer occurs between the chromophore and the metal cation, and the valence electrons localized in the FDC are confined effectively due to the energy blocking action of the metal cations. Combining experimental and theoretical studies on the luminescent MOF system, this work not only gives a rapid and environmentally friendly way to prepare a highly ordered inorganic–organic hybrid system with improved fluorescence properties, but also provides a deep understanding of the electronic structure of the 2D pillared MOF. It is expected that the Zn–FDC MOF can be potentially applied as a polarized fluorescence material.

Received 4th September 2012
Accepted 27th November 2012

DOI: 10.1039/c2tc00591c

www.rsc.org/MaterialsC

Downloaded by Beijing University of Chemical Technology on 07 December 2012
Published on 27 November 2012 on http://pubs.rsc.org | doi:10.1039/C2TC00591C

1 Introduction

The regular arrangement of organic chromophores at the molecular level is of crucial importance to develop high-performance luminescent materials for optoelectronic applications, such as light-emitting diodes,[1] lasers,[2] and sensors.[3] Moreover, the ordered assembly of photoactive molecules is undoubtedly favorable for producing a uniform orientation of transition dipole moments for construction of self-emissive devices with polarized luminescence.[4] In this sense, metal organic frameworks (MOFs), also named as coordination polymers,[5] can be regarded as idealized models to organize highly ordered organic chromophore ligands with the aid of the coordination of metal cations and/or clusters. Recently, MOFs have been paid a great deal of attention because of their facile synthesis and structural diversity in supramolecular solids. As we have known, the development of MOFs with well-defined solid-state luminescence is still in an early stage relative to their studies for gas storage/separation,[6] catalysis,[7] and magnetism.[8] Compared with luminescent MOFs involving the ligand-to-metal charge transfer (LMCT) mechanism, fluorescence with excitation and emission directly from organic ligands can reduce cross-relaxation and thus enhance the photoluminescence efficiency effectively.[9]

Recent advances in mechanochemical synthesis supply an effective and environmentally friendly way to rapidly synthesize ordered MOF materials at room temperature.[10] In such a process, the metal oxides undergo a single-step neutralization with dicarboxylic acids to form MOFs. In addition, it has been known that the introduction of solvents and anions played an important role in determining the topology of the obtained MOF.[11] To achieve a totally ordered arrangement of the organic chromophore, it is preferred to form a two-dimensional (2D) pillared MOF, in which the ligands have the same orientation within the MOF crystal. Such 2D architectures have already been

State Key Laboratory of Chemical Resource Engineering, Beijing University of Chemical Technology, Beijing 100029, P. R. China. E-mail: yandp@mail.buct.edu.cn; yandongpeng001@163.com; Fax: +86-10-64425385; Tel: +86-10-64412131

† Electronic supplementary information (ESI) available: Experimental and simulated XRD profile for Zn–FDC MOF (Fig. S1); atomic coordinates for Zn–FDC (Table S1); the real space and reciprocal space in the first Brillouin Zone (BZ) for Zn–FDC MOF (Fig. S2); total and partial electronic density of states (TDOS and PDOS) profiles for different atoms in Zn–FDC (Fig. S3); TDOS/PDOS and band structure for Zn–FDC MOF with BZ sampled by 4 × 4 × 1 *k*-points (Fig. S4). See DOI: 10.1039/c2tc00591c

Published on 27 November 2012 on http://pubs.rsc.org | doi:10.1039/C2TC00591C
Downloaded by Beijing University of Chemical Technology on 07 December 2012

readily prepared in several Zn-based MOF systems during the mechanosynthesis process.[12]

Fluorenone and its derivatives are an important type of fluorescent molecule with intriguing photophysical performances,[13] which have been studied and applied as new solid-state luminescent materials. Cheetham *et al.* have synthesized MOFs assembled from 9-fluorenone-2,7-dicarboxylate (FDC) in combination with calcium and strontium under hydrothermal conditions at 150 °C for 2 days.[14] Herein, we have selected zinc-based fluorenone dicarboxylate MOF as the model material since the zinc carboxylate MOFs are widespread as functional materials for novel applications. It was observed that 2D pillared Zn–FDC MOFs can be readily formed through a liquid-assisted grinding (LAG) method within 30 minutes. Moreover, the structure, thermal stability and photophysical properties of the Zn–FDC MOF systems were studied by nuclear magnetic resonance (NMR), Fourier-transform infrared (FT-IR) spectra, thermogravimetric analysis (TG) and fluorescence spectroscopy. The as-prepared Zn–FDC MOF exhibited a blue-shifted photoemission, as well as enhanced photoluminescence quantum yield (PLQY) and fluorescence lifetime compared with the pure FDC molecule due to the rigid configuration and highly ordered structure of the chromophore within the inorganic–organic framework. Furthermore, the Zn–FDC MOF thin film showed well-defined polarized photoemission, further confirming the regular arrangement of the organic molecules in the hybrid structure. Furthermore, periodic density functional theoretical (DFT) calculations were employed to probe the geometric and electronic structures of the Zn–FDC MOF system. With a combination of experimental methodology and theoretical study on a MOF system, this work not only provides a feasible and rapid route to construct highly ordered luminescent hybrid structures at room temperature, but also gives a detailed understanding of the energy levels of the 2D pillared MOF. It is also expected that Zn–FDC MOF hybrid systems can be potentially applied in the field of polarized emission materials.

2 Experimental section

2.1 Reagents and materials

9-Fluorenone-2,7-dicarboxylic acid (FDB, 95%) was purchased from J&K Chemical Co. Ltd. Zinc oxide (AR), ethanol (C_2H_5OH, AR), chloroform ($CHCl_3$, AR) and acetone (CH_3COCH_3, AR) were purchased from Sigma Chemical. Co. Ltd. and used without further purification.

2.2 Preparation of Zn–FDC MOF

In a typical liquid-assisted grinding (LAG) experiment, 30 μL of ethanol or chloroform or acetone was added to 200 mg of a solid reactant mixture with the initial ratio of the two compositions (ZnO and FDB) of 1 : 1, respectively. The mixture was ground for 30 min in a Retsch MM200 mill operating at a frequency of 30 Hz. In a standard experiment, two stainless steel balls of 7 mm diameter (1.4 g) were used for grinding. For comparison, the neat-grinding experiment without solvent was also carried out.

2.3 Characterization

The XRD measurements were performed on a Rigaku XRD-6000 diffractometer, using Cu-Kα radiation (λ = 0.15418 nm) at 40 kV, 30 mA, with a scanning rate of 10° min^{-1}, and the 2θ angle ranging from 3 to 50°. Fourier-transform infrared (FT-IR) spectra were recorded on a Bruker Vector 22 using the KBr disk method in the range from 4000 to 600 cm^{-1}, with a resolution of 2 cm^{-1} and an accumulation of 32 scans. Solid-state cross-polarization/magic angle spinning (CP/MAS) ^{13}C nuclear magnetic resonance (NMR) spectra were recorded by a Bruker BioSpin AV 300 MHz at 20 °C with a 4 mm rotor spinning at 5 kHz under a static magnetic field of 9.4 T. ^{13}C spectra were obtained at a frequency of 75.48 MHz with a 5 s relaxation delay and a spectral bandwidth of 350 ppm. TG was measured on a PCT-1A thermal analysis system under ambient atmosphere with a heating rate of 10 °C min^{-1}. The fluorescence spectra were performed on a Hitachi F-7000 FL spectrophotometer with a slit width of 3 nm, excitation at 360 nm and a PMT voltage of 400 V. Fluorescence lifetime measurements were recorded with an Edinburgh Instruments FL 900 fluorometer. The data were calculated with Edinburgh F900 instruments software. Steady-state polarized photoluminescence measurements were recorded with an Edinburgh Instruments' FLS 920 fluorimeter. PLQY and CIE 1931 color coordinates were measured using an HORIBA Jobin-Yvon FluoroMax-4 spectrofluorometer, equipped with an F-3018 integrating sphere.

2.4 Computational methods

The indexing of the peaks in the powder XRD pattern with a long-time scan was performed using the TREOR program[15a] on the Reflex Powder Indexing module in Materials Studio software,[15b] in which the crystal type and approximate lattice parameters can be determined from the peak positions by testing in six common space groups (cubic, hexagonal, tetragonal, orthorhombic, monoclinic, and triclinic). Then, the accurate lattice parameters of the sample were determined by Pawley fitting,[15c] which can give the most likely space groups of the crystal system. The results show that Zn–FDC has a monoclinic lattice with $P2_1/c$ symmetry and the lattice parameters of a = 6.8770 Å, b = 6.3848 Å, c = 28.7917 Å, β = 95.1270°. The symmetry and lattice parameters are close to the crystal of Cd–FDC MOF crystal synthesized by the hydrothermal method,[14b] suggesting the similarity of their structures. The molecular arrangement in the unit cell and the structure solution is further obtained by the use of the simulated annealing method in the Reflex Powder Solve module.[15b] The results of the structure solution step were further improved by Rietveld refinement.[15d] The weighted R-factor (the parameter to measure the similarity between the experimental and the simulated powder patterns) gave R_{wp} = 12.4%. Further theoretical calculations were performed by using the periodic density functional theory (DFT) method on the Dmol3[15e,f] module in the Materials Studio software.[15g] The initial configuration of the Zn–FDC MOF was first fully optimized with fixed positions for the metal atoms by the molecular mechanics method employing a cff91 force field,[15h,i] and then further optimization was implemented by the

 This journal is © The Royal Society of Chemistry 2012

Downloaded by Beijing University of Chemical Technology on 07 December 2012
Published on 27 November 2012 on http://pubs.rsc.org | doi:10.1039/C2TC00591C

Perdew–Wang (PW91)[15j] generalized gradient approximation (GGA) method with double numerical basis sets plus polarization functions (DNP). The core electrons for metals were treated by effective core potentials (ECP). The SCF (self-consistent field) converged criterion was within 1.0×10^{-5} Hartree/atom and convergence criterion for structural optimization was 1.0×10^{-3} Hartree/Bohr. The Brillouin zone is sampled by $3 \times 3 \times 3$ *k*-points, and test calculations reveal that the increase of *k*-points does not affect the results.

3 Results and discussion

3.1 Structural characterization of Zn–FDC MOF

The powder XRD patterns for both neat and liquid-assisted grinding products, as well as their precursors (ZnO and FDB), were shown in Fig. 1. The product by neat grinding of two compositions in a 1 : 1 ratio shows poor crystallinity, which suggests the formation of amorphous structures of the pristine precursors. However, upon adding 30 μL of ethanol or chloroform or acetone, the as-prepared LAG products exhibit different PXRD patterns compared with their precursors, demonstrating that new compositions have formed. In addition, it is noted that the PXRD profiles of the LAG products are very similar, suggesting that the as-prepared samples have the same structure. The main characteristic reflections at 6.19° (1.427 nm), 12.42° (0.712 nm) and 18.71° (0.474 nm) present a good multiple relationship between the basal, second and third-order reflections, indicating the orderly 2D pillared structure within the crystal. To determine the coordination environment of the Zn cations within the MOF, thermogravimetric (TG) analysis was performed on the samples, and the typical TG curve was shown in Fig. 2. A weight loss of 9.8% occurs before 170 °C, which is in agreement with two water molecules as the auxiliary coordination compositions with a Zn atom. With the aid of structural solving and refinement, all the reflections of the as-obtained inorganic–organic hybrid structure can be indexed to a monoclinic lattice with $P2_1/c$ symmetry, in which the adjacent FDC units in the *b* axis direction exhibit an antisymmetric arrangement. The atomic coordinates are tabulated in Table S1 in ESI,† and the simulated XRD pattern of the obtained pillared MOF structure is also consistent with that of the experimental one, as shown in Fig. S1 in ESI.† The typical side-view and top-view profiles for the Zn–FDC MOF are shown in Fig. 3.

To further investigate the structural characterization of the inorganic–organic hybrid materials, FT-IR was recorded for the pristine FDC and Zn–FDC MOF. For the pristine FDC (Fig. 4a), the bands at 1681 and 1614 cm^{-1} are assigned to the characteristic vibrations of C═O in the $-COO^-$ group, and the symmetric stretching vibration band of C–O in the $-COO^-$ at 1413 cm^{-1} can also be observed. The peak at 1469 cm^{-1} can be attributed to the skeleton vibration of phenyl rings. The in-plane bending vibrations of ═C–H in phenyl rings appear at 1239 cm^{-1}. For the Zn–FDC MOF samples (Fig. 4b–d), it is noted that the Zn–FDC materials prepared with different assistant liquids exhibit nearly the same FT-IR spectra. Take the Zn–FDC (acetone) MOF as an example, only one band at 1716 cm^{-1} (Δ = 35 cm^{-1}) was resolved as the vibration of C═O; the bands for

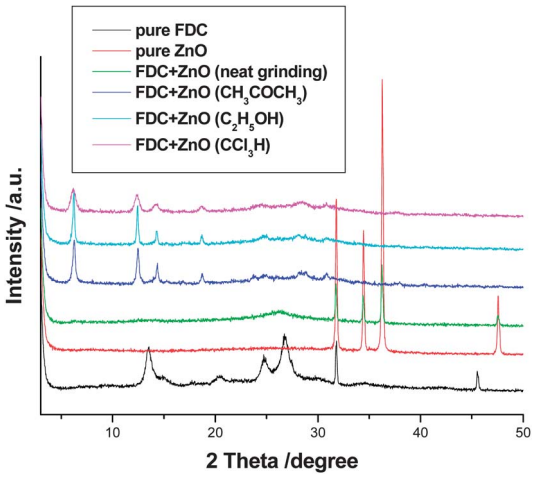

Fig. 1 Powder XRD patterns for the products of neat grinding and LAG reactivity as well as their precursors (ZnO and FDC).

the stretching vibration of the phenyl ring at 1594 and 1553 cm^{-1} can also be observed. Additionally, the symmetric stretching vibration of C–O in the $-COO^-$ is located at 1378 (Δ = −35 cm^{-1}), which is reasonably in agreement with the strong coordination interaction between the carboxylate group and the Zn atom. For the neat grinding sample (Fig. 4e), the most remarkable change is that the vibrations of C═O in the $-COO^-$ group move to 1689 and 1616 cm^{-1}, and this observation may be related to the anchoring of $-COO^-$ groups onto the surface of ZnO particles within the ZnO–FDC mixture.

^{13}C MAS solid-state NMR (Fig. 5) was also performed to probe the molecular packing of the pristine PDC and Zn–FDC MOF. For the pure FDC sample, resonance peaks for sp^2 C_1, C_2, C_3, C_4, C_5, C_6, C_7 and C_8 atoms can be observed at 171.2, 127.1, 133.2, 121.9, 145.8, 130.1, 135.8, and 189.9 ppm, respectively. Upon the formation of the Zn-based MOF material, the NMR peaks became more resolved, suggesting a highly ordered environment for the FDC anions. Moreover, the C_3, C_4 and C_8 atoms undergo a downfield shift to 134.8, 123.7 and 192.1 ppm, indicative of a strong electron-withdrawing effect of the Zn atoms. Specifically, the position of the C_1 atom was split into

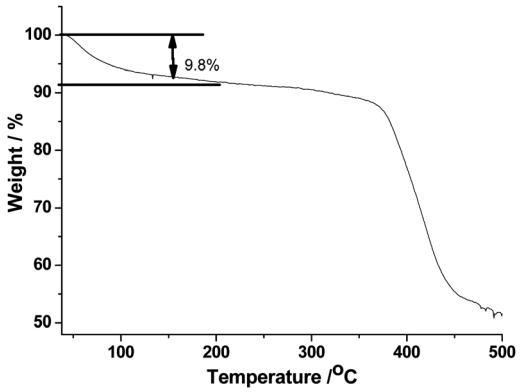

Fig. 2 TG profile for the Zn–FDC MOF.

Downloaded by Beijing University of Chemical Technology on 07 December 2012
Published on 27 November 2012 on http://pubs.rsc.org | doi:10.1039/C2TC00591C

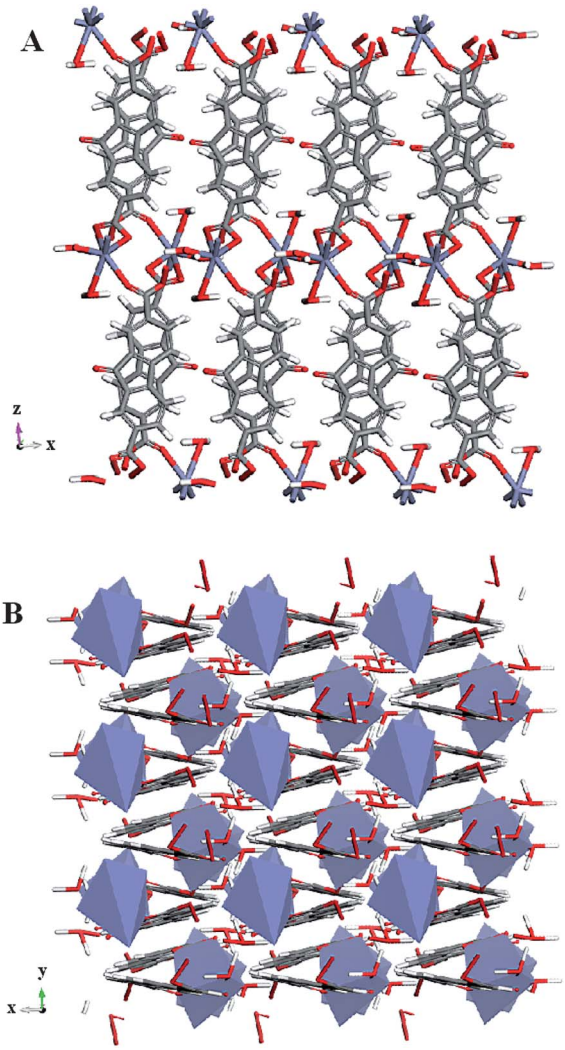

Fig. 3 Zn–FDC MOF structure viewed from (A) [010] and (B) [001] directions.

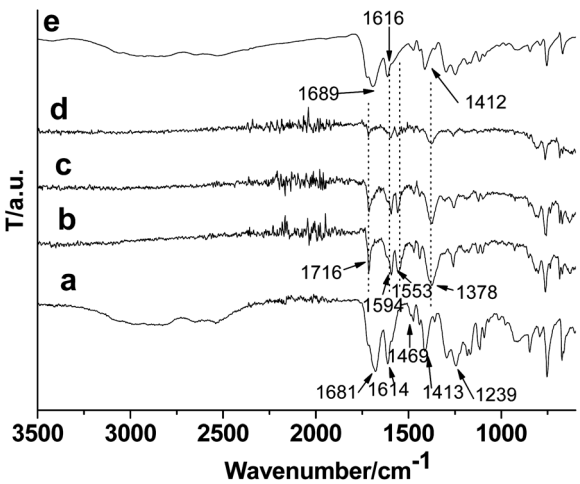

Fig. 4 FT–IR spectra for the pristine FDC (a) and Zn–FDC MOFs (b–d correspond to acetone, chloroform and ethanol as the solvents). (e) corresponds to the neat grinding sample.

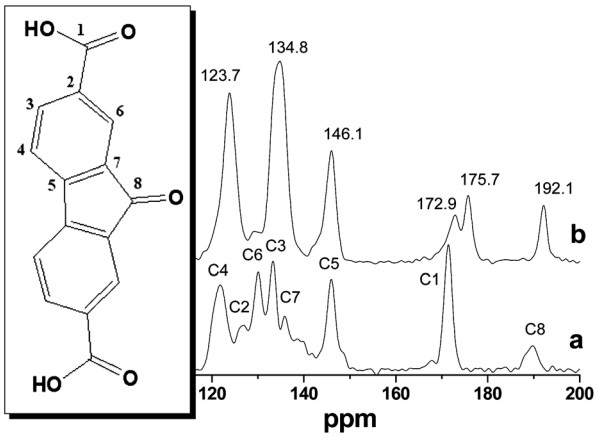

Fig. 5 ^{13}C MAS NMR spectra for (a) the pure FDC, and (b) Zn–FDC MOF.

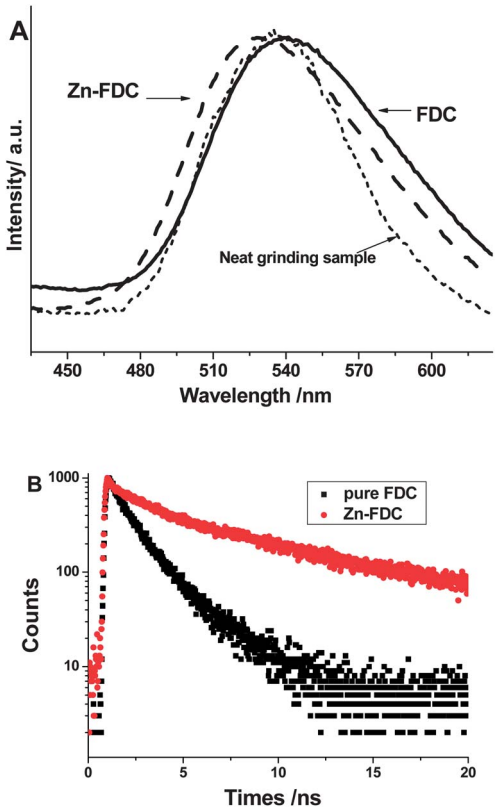

Fig. 6 (A) Fluorescence emission spectra and (B) fluorescence decay curves for pristine FDC and Zn–FDC MOF.

two peaks, suggesting that the two terminal C atoms in the carboxylate exhibit different coordination environments to the Zn atoms within the Zn–FDC MOF, as revealed by the MOF structure.

3.2 Photophysical properties of Zn–FDC MOF

Fig. 6A shows the typical emission spectra of the pure FDC, Zn–FDC MOF and neat grinding samples. Compared with the pure FDC solid sample with the emission peak at 540 nm (CIE 1931

This journal is © The Royal Society of Chemistry 2012

Downloaded by Beijing University of Chemical Technology on 07 December 2012
Published on 27 November 2012 on http://pubs.rsc.org | doi:10.1039/C2TC00591C

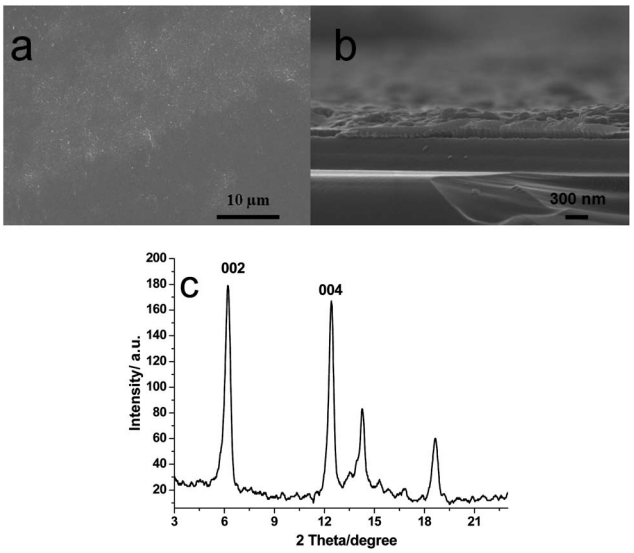

Fig. 7 SEM images for the top-view (a) and side-view (b) images for Zn–FDC MOF; (c) XRD profile for Zn–FDC MOF.

color coordinate: (0.46, 0.53)), the emission position of the Zn–FDC MOF shows a blue-shift at 526 nm (CIE 1931 color coordinate: (0.41, 0.57)); such behavior can be assigned to strong electrostatic interaction between Zn^{2+} and the FDC ligand anions. In this case, the strong electron-withdrawing effect of the Zn^{2+} cations can reduce the electron density in the ligands within the MOF structure, which results in blue-shifted emission. For the neat grinding sample, a blue-shift of 3 nm occurs relative to the pure FDC, which may be related to the interaction between FDC and ZnO particles.

To further study the excited-state properties of both the pure organic compound and the Zn-based MOF materials, samples of pristine FDC and Zn–FDC MOF were studied by detecting their fluorescence decays, and the fluorescence lifetimes can be obtained by fitting the decay profiles with one-exponential form. For the pure FDC (Fig. 6B), the fluorescence lifetime is 1.4 ns; upon formation of the Zn–FDC MOF, the fluorescence lifetime increases to 3.6 ns. Such observation is consistent with the fact that the FDC molecules are restricted and stabilized by the formation of pillared MOF structures, which suppress the thermal vibration and nonradiative relaxation process (such as excitonic coupling and excimer formation). This can be further confirmed by studying the photoluminescence quantum yield (PLQY) of the samples. For the pure FDC, the room-temperature PLQY is 0.80%, while for Zn–FDC MOF with low-wavelength emission, the value is 1.57%. Therefore, it can be concluded that the assembly of FDC to form the Zn-based MOF can improve the luminescence performance effectively.

To the best of our knowledge, although MOF materials with luminescent properties for gas, metal and solvent sensors have been well-documented,[9] polarized emission behavior has been seldom studied. Herein, the highly ordered arrangement of the FDC molecules within the pillared structure further enlightens us to study the polarized properties of the MOF materials. Films of the pure FDC and Zn–FDC MOF were fabricated using a

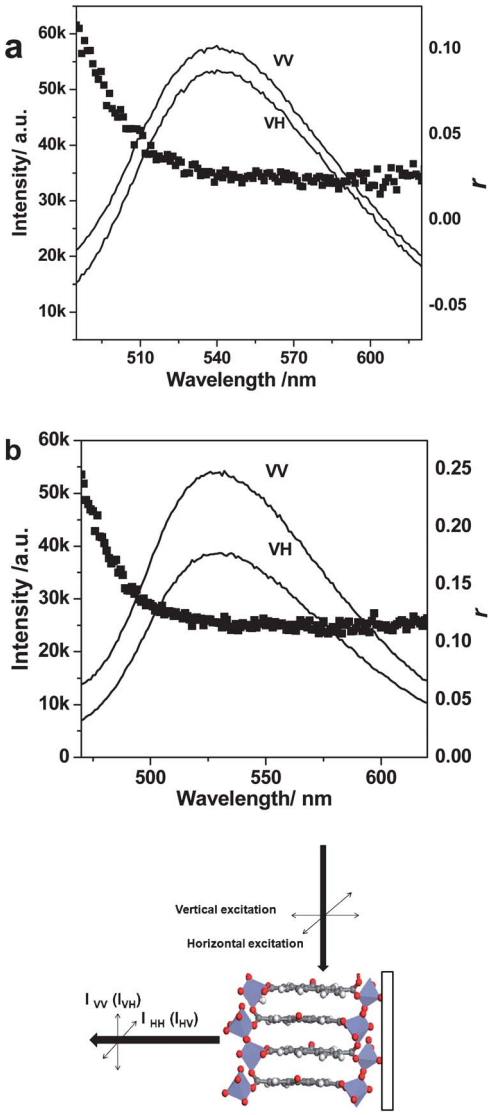

Fig. 8 Photoemission profiles of the VV, VH polarizations and anisotropic value (r) for the pristine FDC (a) and Zn–FDC MOF thin film (b). The scheme corresponds to excitation light with glancing incidence geometry.

solvent evaporation method. A top view of the SEM image (Fig. 7a) for the Zn–FDC MOF film shows that the film surface is continuous and uniform; the thickness can be estimated as about 500 nm by observing the side view of the film, as shown in Fig. 7b. The XRD profile for the Zn–FDC film is shown in Fig. 7c, in which the strong basal reflections (00l) can be observed. The intensity of the (004) reflection is close to that of (002), suggesting c-axis oriented Zn–FDC platelets. By detecting the fluorescence intensity between the parallel and perpendicular to excitation polarized directions (I_{VV} *vs.* I_{VH}), the anisotropic value r can be determined.[16] r can be expressed by the formula:

$$r = \frac{I_{VV} - GI_{VH}}{I_{VV} + 2GI_{VH}},$$

where $G = I_{HV}/I_{HH}$; I_{VH} stands for the photoluminescence intensity obtained with vertical polarized light excitation and

Downloaded by Beijing University of Chemical Technology on 07 December 2012
Published on 27 November 2012 on http://pubs.rsc.org | doi:10.1039/C2TC00591C

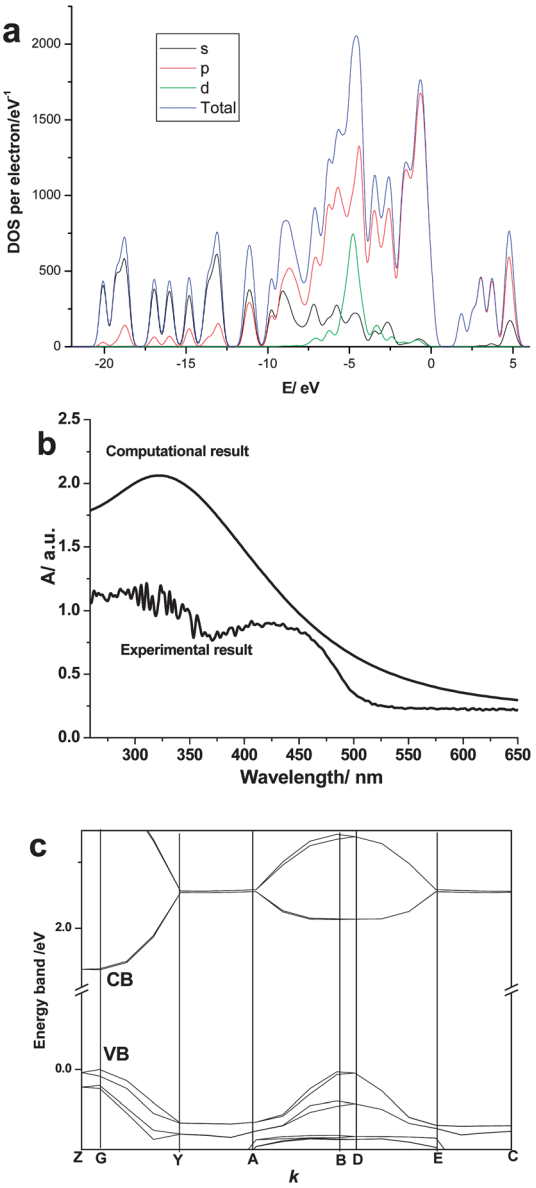

Fig. 9 (a) Total and partial electronic density of states (TDOS and PDOS); (b) experimental and computational UV-vis spectra for Zn–FDC MOF, and (c) band structure for Zn–FDC MOF. *G* (0, 0, 0); *Z* (0, 0, 0.5); *Y* (0, 0.5, 0); *A* (−0.5, 0.5, 0); *B* (−0.5, 0, 0); *D* (−0.5, 0, 0.5); *E* (−0.5, 0.5, 0.5); *C* (0, 0.5, 0.5) are the selected reciprocal points in the first BZ. The energy gap between the conduction band (CB) and valence band (VB) is 1.87 eV.

horizontal polarization detection, and I_{VV}, I_{HH}, I_{HV} are defined in a similar way. A typical measurement setup with incident excitation light along the glancing direction of the thin film was employed to determine the polarized fluorescence (Fig. 8b). Compared with the pure FDB sample (Fig. 8a) with the *r* value in the range of 0.02–0.03, the anisotropy is largely improved in the range 0.10–0.15 for the Zn–FDC MOFs (Fig. 8b). This further confirms that the formation of the pillared MOF structure exhibits a well-oriented and uniformly ordered structure, and the obtained chromophore-containing MOF may also be used as a polarized luminescence material.

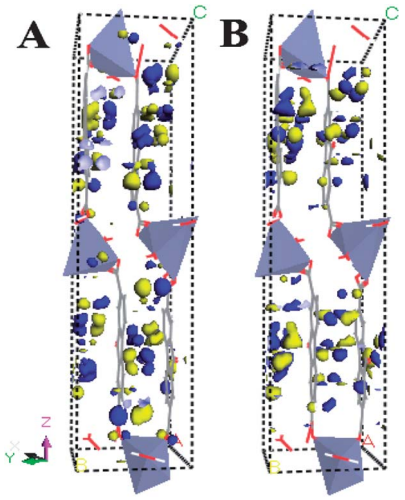

Fig. 10 Frontier orbital profiles for (A) VB and (B) CB of Zn–FDC MOF structure.

3.3 The calculation of the electronic structure

To better understand the electronic structure and energy level characteristics of the luminescent MOF system, periodic density functional theoretical (DFT) calculations were employed on the Zn–FDC structure. Total electronic densities of states (TDOS) and partial electronic densities of states (PDOS) analysis (Fig. 9a and S2 in ESI†) reveal that the valence bands (VB) are distributed on the 2p orbitals of the C and O atoms in FDC, whereas the conduction bands (CB) are mainly dominated by the 2p(π) and 2p(π*) C atomic orbitals in the main fluorenone skeleton. Around the Fermi level, the TDOS mainly consisted of the 2p electrons of the C atoms in the FDC. The 3d and 4s orbitals from the Zn atoms contribute to the TDOS below and above the top of the VB and the bottom of the CB, respectively. Therefore, the photoexcitation process is solely related to the organic chromophore FDC, and no energy or electron transfer occurs between FDC and the Zn atom during the fluorescence process. This can be clearly visualized by observing the frontier orbital profiles of Zn–FDC, as shown in Fig. 10, and such a result further indicates that the valence electrons localized in the FDC are confined effectively due to the energy blocking action of metal cations, which is consistent with the enhancement of the fluorescence lifetime and PLQY values, as evidenced in the experimental section. In addition, the calculated UV-vis spectrum with the maximum absorption band at *ca.* 321 nm is very close to the experimental result (Fig. 9b), confirming the feasibility of DFT calculations for the Zn-based MOF system.

The energy band calculation (Fig. 9c) further shows that the Zn–FDC system exhibits a direct band gap of 1.87 eV between the CB and VB at the *G* point (0, 0, 0) in the first Brillouin Zone (BZ), suggesting that the pillared MOF can be regarded as a hybrid direct semiconductor, which facilitates the improvement of the optical properties of the inorganic–organic material. The energy bands around the Fermi level show nearly complete independence from the *k* electron wave vectors along the ZG line ([001] direction, Fig. S3 in ESI†), indicating a strong valence electron confinement effect in the *c* axis direction. The GY, AB and DE lines (Fig. S3 in ESI†), the *b*-axis direction of the unit

 This journal is © The Royal Society of Chemistry 2012

Published on 27 November 2012 on http://pubs.rsc.org | doi:10.1039/C2TC00591C
Downloaded by Beijing University of Chemical Technology on 07 December 2012

cell, show the highest valence electron dispersion, suggesting electron delocalization occurs between chromophores, which is also consistent with the blue-shift of the photoluminescence spectrum. There is no obvious delocalization of electrons in the AY and CE lines, and such observation is consistent with the fact that no orbital overlap occurs between the neighboring chromophores in the *a*-axis direction of the unit cell. In addition, further calculations with the BZ sampled by $4 \times 4 \times 1$ *k*-points reveal that the selection of *k*-points does not affect the TDOS/PDOS and band structure results (Fig. S4 in ESI†).

4 Conclusion

In summary, 2D pillared Zn-based luminescent MOFs have been prepared by a facile and environmentally friendly liquid-assistant mechanochemical synthesis method. Compared with the pure FDC solid sample, the as-obtained Zn–FDC MOF with a pillared structure shows a blue-shifted photoemission, as well as enhanced PLQY and fluorescence lifetime, suggesting the regular and ordered arrangement of the organic chromophores confined within the MOF reduces the nonradiative relaxation process effectively. Moreover, the Zn–FDC MOF film can exhibit well-defined polarized photoemission with a macroscopic anisotropy of 0.10–0.15 due to the uniform and ordered assembly of FDC. DFT calculations illustrate that the photoexcitation and emission arise from the FDC units in the MOF system, and no energy/electron transfer process occurs. Moreover, the valence electrons localized in the FDC are confined effectively due to the energy blocking effect of metal cations, which facilitates the improvement of the photo-related properties of the organic chromophore. The TDOS/PDOS and energy band analysis further show that the Zn–FDC MOF has directionality in the valence and conduction bands, and the band gap can vary in different directions in the first BZ. It can be anticipated that the strategy here for the assembly of fluorescent molecules into pillared MOF structures can be expanded to other inorganic–organic hybrid systems, in which the improvement of the light-emitting performance for chromophores can be realized.

Acknowledgements

This work was supported by the National Natural Science Foundation of China, the 973 Program (Grant no. 2011CBA00504), 111 Project (Grant no. B07004) and the "Chemical Grid Project" of Beijing University of Chemical Technology.

Notes and references

1 (*a*) M. Strukelj, R. H. Jordan and A. Dodabalapur, *J. Am. Chem. Soc.*, 1996, **118**, 1213; (*b*) R. H. Friend, R. W. Gymer, A. B. Holmes, J. H. Burroughes and R. N. Marks, *Nature*, 1999, **397**, 121; (*c*) Z. Xie, B. Yang, G. Cheng, L. Liu, F. He, F. Shen, Y. Ma and S. Liu, *Chem. Mater.*, 2005, **17**, 1287; (*d*) D. P. Yan, J. Lu, M. Wei, J. B. Han, J. Ma, F. Li, D. G. Evans and X. Duan, *Angew. Chem., Int. Ed.*, 2009, **48**, 3073; (*e*) C. A. Strassert, C.-H. Chien, M. D. G. Lopez, D. Kourkoulos, D. Hertel, K. Meerholz and L. De Cola, *Angew. Chem., Int. Ed.*, 2011, **50**, 946.

2 (*a*) S. L. Oliveira, D. S. Corrêa, L. Misoguti, C. J. L. Constantino, R. F. Aroca, S. C. Zilio and C. R. Mendonça, *Adv. Mater.*, 2005, **17**, 1890; (*b*) F. He, L. L. Tian, X. Y. Tian, H. Xu, Y. H. Wang, W. J. Xie, M. Hanif, J. L. Xia, F. Z. Shen, B. Yang, F. Li, Y. G. Ma, Y. Q. Yang and J. C. Shen, *Adv. Funct. Mater.*, 2007, **17**, 1551.

3 (*a*) J. W. Chung, S.-J. Yoon, S.-J. Lim, B.-K. An and S. Y. Park, *Angew. Chem., Int. Ed.*, 2009, **48**, 7030; (*b*) H. Jiang, P. Taranekar, J. R. Reynolds and K. S. Schanze, *Angew. Chem., Int. Ed.*, 2009, **48**, 4300; (*c*) M. Wang, G. X. Zhang, D. Q. Zhang, D. B. Zhu and B. Z. Tang, *J. Mater. Chem.*, 2010, **20**, 1858; (*d*) M. Boiocchi, L. Fabbrizzi, M. Licchelli, D. Sacchi, M. Vazquez and C. Zampa, *Chem. Commun.*, 2003, 1812; (*e*) N. Yanai, K. Kitayama, Y. Hijikata, H. Sato, R. Matsuda, Y. Kubota, M. Takata, M. Mizuno, T. Uemura and S. Kitagawa, *Nat. Mater.*, 2011, **10**, 787; (*f*) D. P. Yan, J. Lu, M. Wei, D. G. Evans and X. Duan, *J. Mater. Chem.*, 2011, **21**, 13128.

4 (*a*) L. Zang, Y. Che and J. S. Moore, *Acc. Chem. Res.*, 2008, **41**, 1596; (*b*) D. P. Yan, J. Lu, J. Ma, M. Wei, S. H. Qin, L. Chen, D. G. Evans and X. Duan, *J. Mater. Chem.*, 2010, **20**, 5016; (*c*) D. P. Yan, G. O. Lloyd, A. Delori, W. Jones and X. Duan, *ChemPlusChem*, 2012, DOI: 10.1002/cplu.201200245.

5 (*a*) M. Eddaoudi, D. B. Moler, H. Li, B. Chen, T. M. Reineke, M. O'Keeffe and O. M. Yaghi, *Acc. Chem. Res.*, 2001, **34**, 319; (*b*) W. B. Lin, *J. Solid State Chem.*, 2005, **178**, 2486; (*c*) G. Férey, *Chem. Soc.Rev.*, 2008, **37**, 191; (*d*) J. Zhang, R. Liu, P. Feng and X. Bu, *Angew. Chem., Int. Ed.*, 2007, **46**, 8388; (*e*) Y. Xiao, Y. Cui, Q. Zheng, S. Xiang, G. Qian and B. Chen, *Chem. Commun.*, 2010, **46**, 5503; (*f*) N. Yanai, T. Uemura, W. Kosaka, R. Matsuda, T. Kodani, M. Koh, T. Kanemurac and S. Kitagawa, *Dalton Trans.*, 2012, **41**, 4195.

6 (*a*) J. L. C. Rowsell and O. M. Yaghi, *Microporous Mesoporous Mater.*, 2004, **73**, 3; (*b*) M. Eddaoudi, J. Kim, N. Rosi, D. Vodak, J. Wachter, M. O'Keeffe and O. M. Yaghi, *Science*, 2002, **295**, 469; (*c*) L. J. Murray, M. Dincá and J. R. Long, *Chem. Soc. Rev.*, 2009, **38**, 1294; (*d*) K. A. Cychosz, A. G. Wong-Foy and A. J. Matzge, *J. Am. Chem. Soc.*, 2008, **130**, 6938; (*e*) J. R. Li, R. J. Kuppler and H. Zhou, *Chem. Soc. Rev.*, 2009, **38**, 1477.

7 (*a*) J.-X. Jiang, C. Wang, A. Laybourn, T. Hasell, R. Clowes, Y. Z. Khimyak, J. Xiao, S. J. Higgins, D. J. Adams and A. I. Cooper, *Angew. Chem., Int. Ed.*, 2011, **50**, 1072; (*b*) J. S. Seo, D. Wang, H. Lee, S. I. Jun, J. Oh, Y. J. Jeon and K. Kim, *Nature*, 2000, **404**, 982.

8 (*a*) H. A. Habib, J. Sanchiz and C. Janiak, *Dalton Trans.*, 2008, 1734; (*b*) M. Kurmoo, *Chem. Soc. Rev.*, 2009, **38**, 1353; (*c*) D. Maspoch, D. Ruiz-Molina and J. Veciana, *Chem. Soc. Rev.*, 2007, **36**, 770; (*d*) B. V. Harbuzaru, A. Corma, F. Rey, P. Atienzar, J. L. Jorda, H. Garcia, D. Ananias, L. D. Carlos and J. Rocha, *Angew. Chem., Int. Ed.*, 2008, **47**, 1080.

9 (*a*) M. D. Allendorf, C. A. Bauer, R. K. Bhaktaa and R. J. T. Houk, *Chem. Soc. Rev.*, 2009, **38**, 1330; (*b*) P. L. Feng, J. J. Perry IV, S. Nikodemski, B. W. Jacobs,

Downloaded by Beijing University of Chemical Technology on 07 December 2012
Published on 27 November 2012 on http://pubs.rsc.org | doi:10.1039/C2TC00591C

S. T. Meek and M. D. Allendorf, *J. Am. Chem. Soc.*, 2010, **132**, 15487; (*c*) Y. Cui, Y. Yue, G. Qian and B. Chen, *Chem. Rev.*, 2012, **112**, 1126; (*d*) Z.-J. Zhang, W. Shi, Z. Niu, H. Li, B. Zhao, P. Cheng, D. Liao and S. Yan, *Chem. Commun.*, 2011, **47**, 6425.

10 (*a*) S. L. James, C. J. Adams, C. Bolm, D. Braga, P. Collier, T. Friščić, F. Grepioni, K. D. M. Harris, G. Hyett, W. Jones, A. Krebs, J. Mack, L. Maini, A. G. Orpen, I. P. Parkin, W. C. Shearouse, J. W. Steed and D. C. Waddell, *Chem. Soc. Rev.*, 2012, **41**, 413; (*b*) T. Friščić, *Chem. Soc. Rev.*, 2012, **41**, 3493; (*c*) D. P. Yan, A. Delori, G. O. Lloyd, T. Friščić, G. M. Day, W. Jones, J. Lu, M. Wei, D. G. Evans and X. Duan, *Angew. Chem., Int. Ed.*, 2011, **50**, 12483.

11 (*a*) T. Friščić, A. V. Trask, W. Jones and W. D. S. Motherwell, *Angew. Chem., Int. Ed.*, 2006, **45**, 7546; (*b*) T. Friščić, D. G. Reid, I. Halasz, R. S. Stein, R. E. Dinnebier and M. J. Duer, *Angew. Chem., Int. Ed.*, 2010, **49**, 712; (*c*) E. H. H. Chow, F. C. Strobridge and T. Friščić, *Chem. Commun.*, 2010, **46**, 6368; (*d*) W. Yuan, T. Friščić, D. Apperley and S. L. James, *Angew. Chem., Int. Ed.*, 2010, **49**, 3916; (*e*) A. Pichon, A. Lazuen-Garay and S. L. James, *CrystEngComm*, 2006, **8**, 211; (*f*) M. R. Caira, L. R. Nassimbeni and A. F. Wildervanck, *J. Chem. Soc., Perkin Trans. 2*, 1995, 2213; (*g*) A. M. Flock, C. M. M. Reucher and C. Bolm, *Chem.–Eur. J.*, 2010, **16**, 3918.

12 T. Friščić and L. Fábian, *CrystEngComm*, 2009, **11**, 743.

13 (*a*) J. R. Heldt, J. Heldt, M. Józefowicz and J. Kamiński, *J. Fluoresc.*, 2001, **11**, 65; (*b*) Q. Yue, L. Yan, J.-Y. Zhang and E.-Q. Gao, *Inorg. Chem.*, 2010, **49**, 8647.

14 (*a*) J. D. Furman, A. Y. Warner, S. J. Teat, A. A. Mikhailovsky and A. K. Cheetham, *Chem. Mater.*, 2010, **22**, 2255; (*b*) J. D. Furman, B. C. Melot, S. J. Teat, A. A. Mikhailovsky and A. K. Cheetham, *Phys. Chem. Chem. Phys.*, 2011, **13**, 7622.

15 (*a*) P.-E. Werner, L. Eriksson and M. Westdahl, *J. Appl. Crystallogr.*, 1985, **18**, 367; (*b*) *Reflex Module, MS Modeling, Version 2.2*, Accelrys Inc., San, Diego, CA, 2003; (*c*) A. J. Markvardsen, W. I. F. David, J. C. Johnson and K. Shankland, *Acta Crystallographica Section A Foundations of Crystallography*, 2000, **57**, 47; (*d*) R. A. Young, *The Rietveld Method, IUCr Monographies of Crystallography 5*, Oxford University Press, Oxford, 1993; (*e*) B. Delley, *J. Chem. Phys.*, 1990, **92**, 508; (*f*) B. Delley, *J. Chem. Phys.*, 2000, **113**, 7756; (*g*) *Dmol3 Module, MS Modeling, Version 2.2*, Accelrys Inc., San, Diego, CA, 2003; (*h*) J. R. Maple, M.-J. Hwang, T. P. Stockfisch, U. Dinur, M. Waldman, C. S. Ewig and A. T. Hagler, *J. Comput. Chem.*, 1994, **15**, 162; (*i*) D. P. Yan, J. Lu, M. Wei, H. Li, J. Ma, F. Li, D. G. Evans and X. Duan, *J. Phys. Chem. A*, 2008, **112**, 7671; (*j*) J. P. Perdew, J. A. Chevary, S. H. Vosko, K. A. Jackson, M. R. Pederson, D. J. Singh and C. Fiolhais, *Phys. Rev. B: Condens. Matter*, 1992, **46**, 6671.

16 (*a*) B. Valeur, *Molecular Fluorescence: Principles and Applications*,Wiley-VCH Verlag GmbH, 2001; (*b*) D. P. Yan, J. Lu, J. Ma, M. Wei, D. G. Evans and X. Duan, *Phys. Chem. Chem. Phys.*, 2010, **12**, 15085.

 This journal is © The Royal Society of Chemistry 2012